*Nanomed Res J 9(1):71-79, Winter 2024*

RESEARCH ARTICLE

# DFT Studies on the performance of Pristine and Si-doped Fullerenes ($C_{20}$ and $SiC_{19}$) as Adsorbent and Sensor for Methyl Paraben

***Mohammad Reza Jalali Sarvestani[1], Mahnaz Qomi[2,3], and Simin Arabi[4]****

[1] *Young Researchers and Elite Club, Yadegar-e-Imam Khomeini (RAH) Shahr-e-Rey Branch, Islamic Azad University, Tehran, Iran*

[2] *Active Pharmaceutical Ingredients Research Center (APIRC), Tehran Medical Sciences, Islamic Azad University, Tehran, Iran*

[3] *Department of Medicinal Chemistry, Faculty of Pharmacy, Tehran Medical Sciences, Islamic Azad University, Tehran, Iran*

[4] *Department of Chemistry, Safadasht Branch, Islamic Azad University, Tehran, Iran*

**ARTICLE INFO**

***Article History:***
*Received 21 Dec 2023*
*Accepted 16 Mar 2024*
*Published 01 Apr 2024*

***Keywords:***
*Fullerene*
*Methyl paraben*
*Adsorption*
*Density functional theory*
*Thermochemistry*

**ABSTRACT**

The research investigated the performances of pristine and Si-doped fullerenes ($C_{20}$ and $SiC_{19}$) as an adsorbent and sensor for the removal and detection of methyl paraben (MP) using density functional theory computations. The results indicated that MP interaction with $C_{20}$ is experimentally impossible, endothermic, and non-spontaneous, suggesting that $C_{20}$ is not an effective adsorbent for the removal of MP. On the other hand, MP adsorption on the surface of $SiC_{19}$ is experimentally feasible, exothermic, spontaneous, and thermodynamically reversible, indicating that $SiC_{19}$ could be a potential adsorbent for the removal of MP. The study also scrutinized the effects of water as the solvent and changing temperature on the thermodynamic parameters. The findings revealed that both parameters do not have any meaningful effects on the interactions in the case of both adsorbents. Additionally, the Frontier Molecular Orbital (FMO) analysis showed that $SiC_{19}$ is more conductive than $C_{20}$. Moreover, the bandgap of $C_{20}$ did not experience significant changes during the adsorption process, while the bandgap of $SiC_{19}$ decreased from 5.840 eV to 3.270 eV. This implies that Si-doped fullerene can be utilized as a good electrocatalytic modifier for the electrochemical detection of methyl paraben. In conclusion, the research provides valuable insights into the potential use of Si-doped fullerene ($SiC_{19}$) as an effective adsorbent and sensor for the removal and detection of methyl paraben.

**How to cite this article**
*Jalali Sarvestani MR, Qomi M, Arabi S. DFT Studies on the performance of Pristine and Si-doped Fullerenes ($C_{20}$ and $SiC_{19}$) as Adsorbent and Sensor for Methyl Paraben. Nanomed Res J, 2024; 9(1): 71-79. DOI: 10.22034/nmrj.2024.01.008*

## INTRODUCTION

Methylparaben (MP, Fig. 1) is a synthetic compound widely used as an antimicrobial preservative in personal care products, cosmetics, food, and pharmaceuticals. It is an ester of para-hydroxybenzoic acid and methanol and belongs to a class of chemicals known as parabens, including ethylparaben, propylparaben, and butylparaben. These compounds are added to products to prevent the growth of bacteria, mold, and yeast, extending the shelf life of the product [1]. Methylparabens have poor biodegradability and can harm human health and the environment. There is a need for new analytical methods to detect and remove them from environmental samples to ensure safety. Researchers are making efforts to address this concern and mitigate the risks of methylparaben contamination [2]. In recent years, different methods such as electrochemical oxidation [3], photolysis [4], Advanced Oxidation Processes [5-7], photocatalytic ozonation [8-10], Fenton

* Corresponding Author Email: *siminarabi1354@yahoo.com*

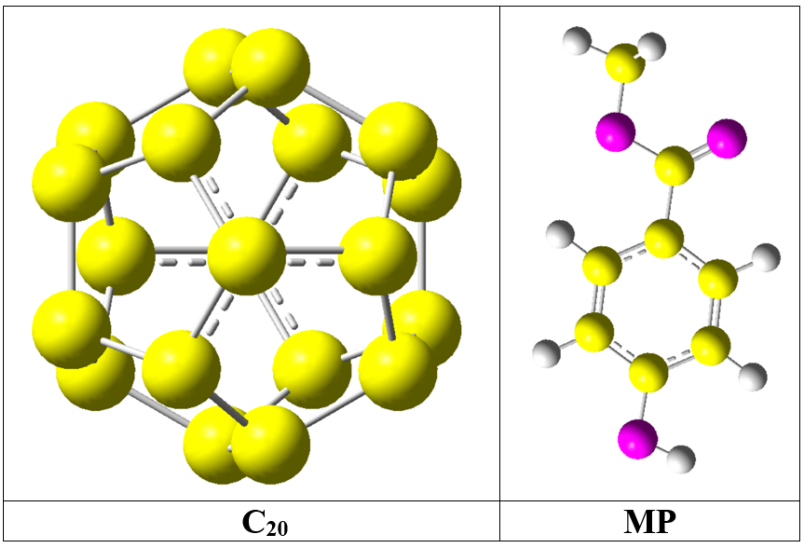


Fig. 1. The optimized structures of fullerene (C20) and MP (yellow: carbon, white: hydrogen, purple: oxygen)

oxidation [11], sonochemical degradation [12] and nanofiltration [13] have been used for the removal of parabens from wastewater. However, because of some difficulties found in the use of these methods such as high consumption of energy, treatment of a large volume of sewage, separation and reuse of photocatalyst particles, high operation cost and sedimentation in the membrane and disposal problems, the adsorption process as compared with other traditional methods because of its simple design, easy access, high efficiency and selectivity, low maintenance cost, highly economic benefits, rapidness, and less requirement of control systems seems to be an excellent technique for parabens removal [14,15]. The development of a cost-effective, reusable adsorbent with high capacity and selectivity in difficult conditions remains a significant challenge. Research is underway to explore various materials and technologies, testing various compounds and surface modifications to improve performance while balancing considerations of cost, environmental impact, and scalability. Despite the difficulties, advancements in material science and chemical engineering offer promise for effective adsorbents. Collaboration among experts is essential for driving innovation in adsorbent development. There are several methods for determining the presence of parabens in various products such as foods, cosmetics, and pharmaceuticals. Some of the commonly used methods include high-performance liquid chromatography [16,17], capillary electrophoresis [18], gas chromatography [19], and ultraviolet-visible (UV-Vis) spectrophotometric [20] techniques. The mentioned techniques suffer from various drawbacks, including expensive and complex instrumentation, time-consuming, consumption of high amounts of toxic organic solvent, and the need to skilled operators to perform sample preparation and analysis steps [21,22]. Electrochemical sensors present numerous benefits when compared to other types of sensors. Their portability, user-friendly nature, and cost-effectiveness in terms of instrumentation are notable advantages. Moreover, they boast high selectivity and sensitivity, enabling precise and dependable measurements. The rapid analysis procedures of electrochemical sensors contribute to their efficiency in conducting quick tests and producing results. Their capability to test opaque and colored samples also adds versatility across various testing environments. Altogether, these advantages position electrochemical sensors as a preferred choice for applications where portability, ease of use, and cost-efficiency hold significant importance [23,24]. These characteristics make electrochemical sensors an ideal alternative to traditional analytical techniques. So, the initial and significant step in the development of a new electrochemical sensor and an adsorbent for the detection and removal of an analyte is to find an appropriate modifier that well and selectively interacts with the desired compound [25,26]. This interaction should result in a significant change in

the electrical conductivity of the sensing material, enabling accurate detection and measurement of the analyte. On the other hand, Fullerenes are molecules composed entirely of carbon, typically shaped like spheres, ellipsoids, or tubes. Fullerene 20, also known as $C_{20}$, with a cage like chemical structure is the smallest fullerene which consists solely of 12 pentagons. $C_{20}$ exhibits reactivity as a result of its non-spherical aromaticity, low energy differential, and inherent instability. Exploring its cycloaddition reactions with other π-systems could offer valuable insights into its reactivity and potential applications across diverse fields. Gaining comprehension of these interactions could lead to advancements in scientific understanding and the creation of new materials and technologies [27,28]. Fullerenes, a type of carbon molecules, have recently shown promise as gas sensors. Each carbon atom in a fullerene functions as a surface atom, resulting in highly sensitive electron transport. This sensitivity makes fullerenes attractive for gas detection across various applications, with their unique structure and electronic properties enhancing gas sensing technologies. As research advances, fullerene-based gas sensors hold potential for improving environmental monitoring, industrial safety, and healthcare diagnostics [30]. The potential applications of carbonaceous nanostructures in sensing and adsorption of MP have not been explored using density functional theory (DFT) methods. To address this gap, we conducted DFT computations to investigate the adsorption of MP on pristine and Si-doped fullerenes ($C_{20}$ and $SiC_{19}$) as potential sensors and adsorbents. Our study aimed to understand the adsorption characteristics and sensing capability of these nanostructures towards MP, providing valuable insights for potential practical applications in environmental monitoring and detection of MP.

## COMPUTATIONAL DETAILS

The $C_{20}$, $SiC_{19}$, MP, and their combinations were designed using GuassView 6 [30] and Nanotube Modeler 1.3.0.3 [31] software versions, and then geometric optimization was performed for each structure. Subsequently, the optimized structures underwent various computations, including infra-red (IR), and frontier molecular orbital (FMO). The density functional theory (DFT) method, particularly the B3LYP/6-31G (d) level of theory, was consistently applied using Gaussian 16 [32] software version. This level of theory was chosen due to its prior acceptance and consistent alignment with experimental findings, as well as its proven reliability in predicting experimental results. This selection was made to ensure that the theoretical calculations closely correspond to the actual observations, thereby enhancing the validity and applicability of the research findings [33-38]. The study conducted computations in both vacuum and aqueous phases employing the CPCM [39] solvation method. Temperatures varying from 298 K to 318 K were examined, focusing on MP adsorption onto an adsorbent material. The following process was scrutinized:

$$\text{MP} + \text{Adsorbent} \rightarrow \text{MP-Adsorbent} \quad (1)$$

The computed thermodynamic and FMO parameters were calculated as explained in [40-46].

## RESULTS AND DISCUSSION

*MP interaction with pristine fullerene ($C_{20}$)*

The initial and optimized structures of the MP-$C_{20}$ complexes are depicted in Fig. 2. The study investigated the interaction of MP with $C_{20}$ at two different configurations to determine the most stable one. In A-Conformer, the nanostructure is positioned near the methyl ester group of MP, while in B-conformer, the adsorbent is situated near the benzene ring of MP in a parallel orientation. Following geometrical optimization, it was observed that the adsorbate moved away from the adsorbent in both configurations, indicating relatively weak interactions between the two [33]. The adsorption energies listed in Table 1 are all positive, indicating that the adsorption process is not feasible in experimental conditions [34]. The influence of water as a solvent on the adsorption energies was also examined, and it was found that it does not affect the interactions [35]. This suggests that the presence of water does not play a significant role in altering the adsorption energies. These findings are important for understanding the practical limitations of the adsorption process and provide valuable insights for further research in this area. After performing geometrical optimizations, the scrutinized structure underwent IR computations, and the resulting minimum and maximum frequencies are listed in Table 1. It is evident from the computed frequencies that all values are positive, indicating that all investigated structures represent true local minimums. This outcome confirms the stability of the structures

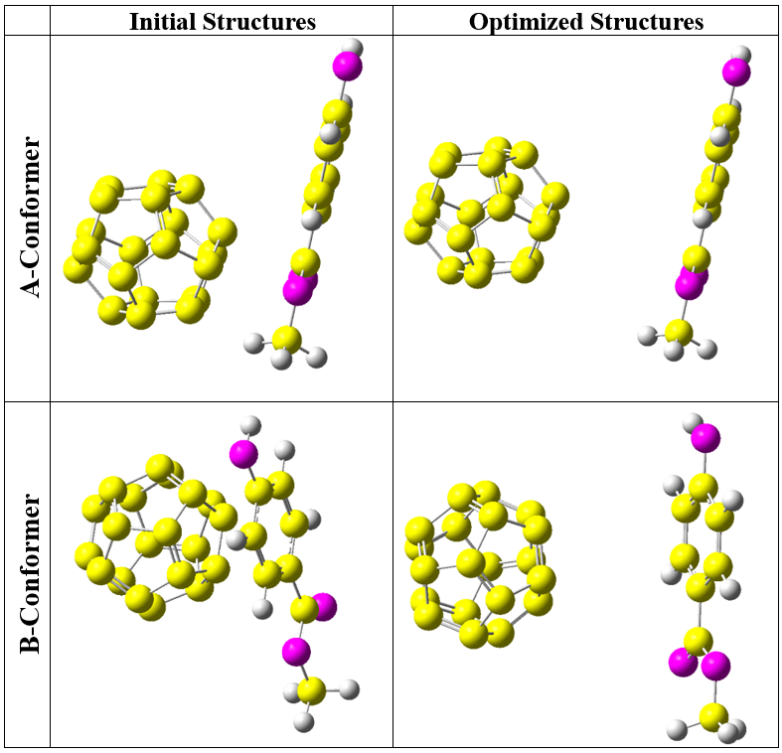


Fig. 2. The initial and optimized structures of fullerene (C20) and MP complexes (yellow: carbon, white: hydrogen, purple: oxygen)

Table 1. Structural properties of MP, $C_{20}$ and their complexes

| NO | Total electronic energy (a.u) | Adsorption energy (kJ/mol) | Zero-point energy (kJ/mol) | $\nu_{min}$ ($cm^{-1}$) | $\nu_{max}$ ($cm^{-1}$) | Dipole moment (Deby) |
|---|---|---|---|---|---|---|
| MP (Vacuum) | -525.407 | --- | 376.980 | 53.186 | 4261.516 | 0.720 |
| MP (Water) | -525.403 | --- | 374.510 | 49.178 | 4262.981 | 0.735 |
| $C_{20}$ (Vacuum) | -747.196 | --- | 325.130 | 262.134 | 1689.950 | 0.000 |
| $C_{20}$ (Water) | -747.198 | --- | 326.340 | 2.1456 | 4263.432 | 0.010 |
| A-Conformer (Vacuum) | -1272.602 | 3.046 | 796.280 | 1.884 | 4261.946 | 0.780 |
| A-Conformer (Water) | -1272.597 | 10.502 | 801.260 | 2.3987 | 4262.1983 | 0.810 |
| B-Conformer (Vacuum) | -1272.599 | 11.694 | 796.850 | 1.831 | 4262.197 | 0.770 |
| B-Conformer (Water) | -1272.600 | 2.660 | 799.710 | 1.9320 | 4262.9818 | 1.090 |

under scrutiny. [36]. The dipole moment values are included in Table 1, and the data clearly indicate that there are no significant changes in the dipole moment values when MP is adsorbed onto the surface of $C_{20}$. This suggests that the solubility of MP remains relatively unchanged during the adsorption process [37].

The reported thermodynamic parameters in Table 2 indicate that the interaction between MP and $C_{20}$ is endothermic and non-spontaneous, as shown by the positive values of $\Delta H_{ad}$ and $\Delta G_{ad}$. This is further confirmed by the low values of the thermodynamic equilibrium constants [40]. The study also examined the influence of temperature and solvent on the thermodynamic parameters, revealing that neither of these factors had a significant impact on the interactions [41]. Additionally, the negative values of $\Delta S_{ad}$ indicate that the adsorption process is not favorable in terms of entropy [42]. These findings provide valuable insights into the nature of the adsorption process and its thermodynamic characteristics.

Table 2. Thermodynamic parameters of adsorption process as a function of temperature

| NO | $\Delta H_{ad}$ (kJ/mol) | $\Delta G_{ad}$ (kJ/mol) | $\Delta S_{ad}$ (J/mol) | $K_{th}$ |
|---|---|---|---|---|
| A-Conformer-Vacuum-298 | 5.756 | 80.152 | -104.567 | $9.062\times10^{-15}$ |
| A-Conformer-Vacuum-308 | 5.911 | 82.896 | -104.329 | $8.865\times10^{-15}$ |
| A-Conformer-Vacuum-318 | 6.066 | 85.192 | -104.091 | $1.029\times10^{-14}$ |
| A-Conformer-Water-298 | 6.221 | 88.340 | -103.853 | $3.332\times10^{-16}$ |
| A-Conformer-Water-308 | 6.376 | 91.002 | -103.615 | $3.746\times10^{-16}$ |
| A-Conformer-Water-318 | 6.531 | 93.701 | -103.377 | $4.125\times10^{-16}$ |
| B-Conformer-Vacuum-298 | 6.686 | 96.345 | -103.139 | $1.319\times10^{-17}$ |
| B-Conformer-Vacuum-308 | 6.841 | 99.018 | -102.901 | $1.640\times10^{-17}$ |
| B-Conformer-Vacuum-318 | 6.996 | 101.756 | -102.663 | $1.963\times10^{-17}$ |
| B-Conformer-Water-298 | 7.151 | 104.503 | -102.425 | $4.908\times10^{-19}$ |
| B-Conformer-Water-308 | 7.306 | 107.265 | -102.187 | $6.559\times10^{-19}$ |
| B-Conformer-Water-318 | 7.485 | 108.452 | -101.949 | $1.561\times10^{-18}$ |

Table 3. FMO parameters for MP, $C_{20}$ and their complexes

| NO | $E_{HOMO}$ (eV) | $E_{LUMO}$ (eV) | Eg (eV) | %ΔEg | η (eV) | μ (eV) | ω (eV) | ΔNmax (eV) |
|---|---|---|---|---|---|---|---|---|
| MP | -6.970 | 5.980 | 12.950 | --- | 6.475 | -0.495 | 0.019 | 0.076 |
| $C_{20}$ | -4.350 | 2.850 | 7.200 | --- | 3.600 | -0.750 | 0.078 | 0.208 |
| A-Conformer | -4.480 | 3.260 | 7.740 | 7.500 | 3.870 | -0.610 | 0.048 | 0.158 |
| B-Conformer | -4.490 | 3.370 | 7.860 | 9.167 | 3.930 | -0.560 | 0.040 | 0.142 |

The provided data in Table 3 clearly demonstrate the impact of MP adsorption on the properties of $C_{20}$. The bandgap of $C_{20}$ shifts from 7.200 eV to 7.740 and 7.860 eV for A and B conformers, respectively, indicating a slight change in bandgap during the adsorption process. This suggests that pristine fullerene may not be an effective electrocatalyst modifier for MP detection. Furthermore, the chemical hardness of MP decreases significantly upon interaction with $C_{20}$, implying increased chemical reactivity. The negative values of chemical potential confirm the thermodynamic stability of the studied structures. Additionally, the electrophilicity and maximum transferred charge capacity of MP increase noticeably after adsorption on the $C_{20}$ surface, indicating a higher tendency for electron absorption. Overall, these findings suggest that MP-$C_{20}$ complexes exhibit enhanced chemical reactivity compared to pure MP without a nanostructure.

*MP Interaction with Si-doped fullerene ($SiC_{19}$)*

As the provided data show clearly pristine fullerene did not have an appropriate interaction with MP. Besides, its bandgap did not experience a tangible variation implying this nanostructure cannot be an appropriate sensor or adsorbent for the detection and removal of MP. Therefore, we doped the fullerene with silicon to check is $SiC_{19}$ performs better than $C_{20}$ or not. The initial and optimized structures of MP- $SiC_{19}$ complexes are given in Fig. 3. As it is obvious, in Si-A-conformer, $SiC_{19}$ is placed near the methyl ester group of MP and in Si-B-Conformer, the nanostructure is placed parallelly near the benzene ring of MP. As the optimized structures in Fig. 3 show clearly, after geometrical optimizations, sharp structural distortions occur in the adsorbent and adsorbate implying strong interactions exist between them [33].

The values of total electronic energy and adsorption energies are reported in Table 4. As it is obvious, Si-B-Conformer has lower energy than Si-A-Conformer implying this configuration is more energetically stable [34]. The negative values of adsorption energies show the adsorption process is experimentally possible. The values of minimum and maximum IR frequencies in Table 4 show none of the studied structures have negative frequencies and all of them are true local minimums [35]. The calculated dipole moment values showed MP- $SiC_{19}$ complexes have higher values of dipole moment in

comparison to pure MP without nanostructures implying the solubility of MP in polar solvents can enhance after its interaction with $SiC_{19}$ [36].

The thermodynamic parameters of MP adsorption process on the surface of $SiC_{19}$ is reported in Table 5. As can be seen, the values of $\Delta H_{ad}$ and $\Delta G_{ad}$ is negative for both studied configurations indicating MP adsorption process is exothermic and experimentally feasible [37]. The low values of thermodynamic parameters show MP interaction with $SiC_{19}$ is reversible and equilibrium. The impact of changing temperature and the presence of water as the solvent. The negative values of $\Delta S_{ad}$ show the interaction process is inappropriate in terms of entropy which can be due to the aggregation of complexes [38].

The FMO parameters of the adsorption process are detailed in Table 6, revealing significant changes in the properties of $SiC_{19}$ and MP upon interaction. The bandgap of $SiC_{19}$ is reported to be 5.840 eV, indicating higher conductivity compared to $C_{20}$ with a bandgap of 7.200 eV. Upon adsorption of MP on the surface of $SiC_{19}$, the bandgap decreases by 24.658% and 44.007% for Si-A and Si-B conformers, respectively. This suggests a significant impact on the electronic properties of the system. Additionally, the chemical hardness of MP decreases substantially after adsorption, indicating increased chemical reactivity in the MP-$SiC_{19}$ complexes. Furthermore, the negative values of chemical potential indicate thermodynamic stability for all studied structures. Interestingly, the electrophilicity and maximum transferred charge capacity of MP increase notably after adsorption on Si-doped fullerene, highlighting its enhanced electron-absorbing tendency. These findings shed light on the potential applications of MP-$SiC_{19}$ complexes in electronic devices and catalysis.

Table 4. Structural properties of MP, $SiC_{19}$ and their complexes

| NO | Total electronic energy (a.u) | Adsorption energy (kJ/mol) | Zero-point energy (kJ/mol) | $\nu_{min}$ ($cm^{-1}$) | $\nu_{max}$ ($cm^{-1}$) | Dipole moment (Deby) |
|---|---|---|---|---|---|---|
| MP (Vacuum) | -525.407 | --- | 376.980 | 53.186 | 4261.516 | 0.720 |
| MP (Water) | -525.403 | --- | 374.510 | 49.178 | 4262.981 | 0.735 |
| $SiC_{19}$ (Vacuum) | -995.394 | --- | 315.490 | 235.620 | 1657.216 | 3.92 |
| $SiC_{19}$ (Water) | -995.401 | --- | 316.510 | 233.487 | 1658.119 | 4.010 |
| Si-A-Conformer (Vacuum) | -1520.842 | -106.246 | 782.980 | 15.663 | 4267.144 | 10.420 |
| Si-A-Conformer (Water) | -1520.848 | -104.574 | 781.200 | 17.542 | 4268.103 | 11.680 |
| Si-B-Conformer (Vacuum) | -1520.871 | -182.386 | 795.390 | 11.897 | 3743.530 | 3.310 |
| Si-B-Conformer (Water) | -1520.868 | -157.084 | 796.530 | 12.991 | 3854.576 | 4.870 |

Table 5. Thermodynamic parameters of adsorption process as a function of temperature

| NO | $\Delta H_{ad}$ (kJ/mol) | $\Delta G_{ad}$ (kJ/mol) | $\Delta S_{ad}$ (J/mol) | $K_{th}$ |
|---|---|---|---|---|
| Si-A-Conformer-Vacuum-298 | -86.110 | -11.714 | -110.245 | $1.128\times10^{+02}$ |
| Si-A-Conformer-Vacuum-308 | -85.955 | -26.395 | -109.926 | $2.981\times10^{+04}$ |
| Si-A-Conformer-Vacuum-318 | -85.800 | -23.679 | -109.607 | $7.725\times10^{+03}$ |
| Si-A-Conformer-Water-298 | -85.645 | -20.952 | -109.288 | $4.686\times10^{+03}$ |
| Si-A-Conformer-Water-308 | -85.490 | -18.290 | -108.969 | $1.260\times10^{+03}$ |
| Si-A-Conformer-Water-318 | -85.335 | -15.591 | -108.650 | $3.629\times10^{+02}$ |
| Si-B-Conformer-Vacuum-298 | -162.249 | -87.854 | -108.331 | $2.467\times10^{+15}$ |
| Si-B-Conformer-Vacuum-308 | -162.094 | -102.535 | -108.012 | $2.406\times10^{+17}$ |
| Si-B-Conformer-Vacuum-318 | -161.939 | -99.819 | -107.693 | $2.450\times10^{+16}$ |
| Si-B-Conformer-Water-298 | -161.784 | -97.091 | -107.374 | $1.025\times10^{+17}$ |
| Si-B-Conformer-Water-308 | -161.629 | -94.429 | -107.055 | $1.017\times10^{+16}$ |
| Si-B-Conformer-Water-318 | -161.474 | -91.730 | -106.736 | $1.151\times10^{+15}$ |

Table 6. FMO parameters for MP, $SiC_{19}$ and their complexes

| NO | $E_{HOMO}$ (eV) | $E_{LUMO}$ (eV) | Eg (eV) | %ΔEg | η (eV) | μ (eV) | ω (eV) | ΔNmax (eV) |
|---|---|---|---|---|---|---|---|---|
| MP | -6.970 | 5.980 | 12.950 | --- | 6.475 | -0.495 | 0.019 | 0.076 |
| $SiC_{19}$ | -3.870 | 1.970 | 5.840 | --- | 2.920 | -0.950 | 0.155 | 0.325 |
| Si-A-Conformer | -2.650 | 1.750 | 4.400 | -24.658 | 2.200 | -0.450 | 0.046 | 0.205 |
| Si-B-Conformer | -2.530 | 0.740 | 3.270 | -44.007 | 1.635 | -0.895 | 0.245 | 0.547 |

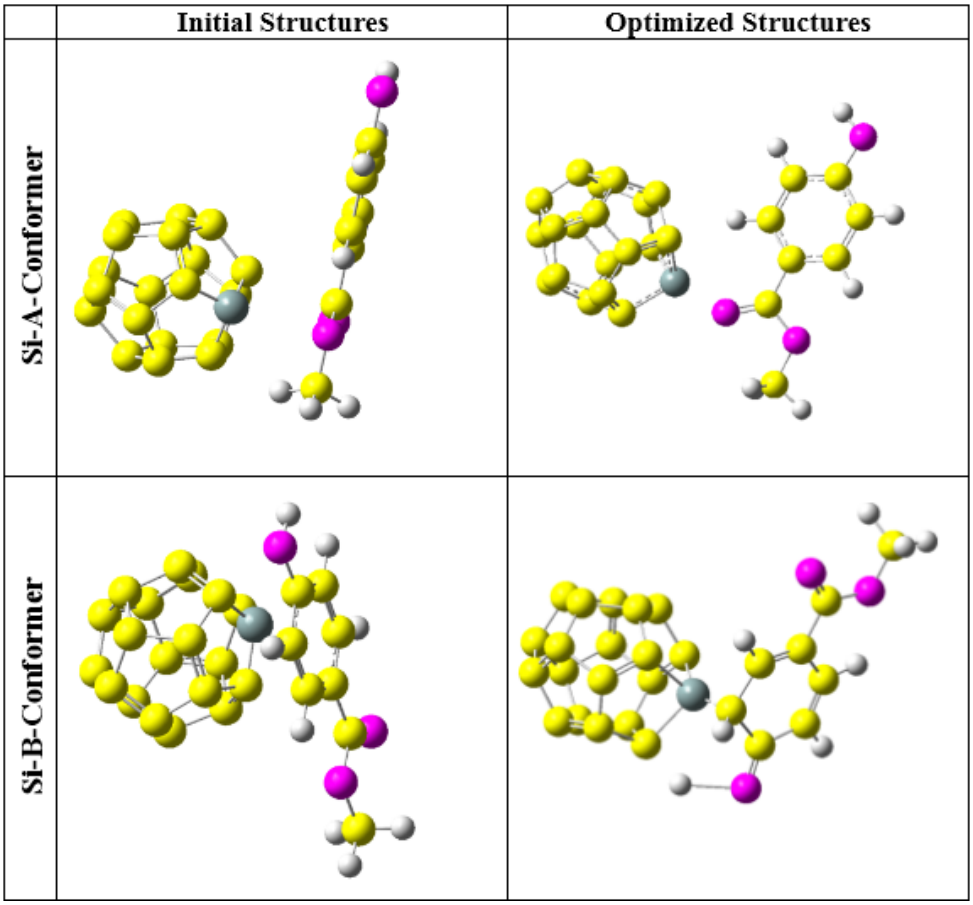


Fig. 3. The initial and optimized structures of Si-doped fullerene (SiC19) and MP complexes (yellow: carbon, white: hydrogen, purple: oxygen, gray: silicon)

## CONCLUSION

The research conducted focused on investigating the performance of pristine and Si-doped fullerenes, specifically $C_{20}$ and $SiC_{19}$, as an adsorbent and sensor for the removal and detection of methyl paraben (MP) using density functional theory computations. The results obtained indicated that the interaction of MP with $C_{20}$ is experimentally impossible, endothermic, and non-spontaneous. On the other hand, MP adsorption on the surface of $SiC_{19}$ was found to be experimentally feasible, exothermic, spontaneous, and thermodynamically reversible. This implies that $C_{20}$ is not an effective adsorbent for the removal of MP. Furthermore, the effects of water as the solvent and changes in temperature on the thermodynamic parameters were scrutinized. The findings revealed that both parameters do not have any significant effects on the interactions in the case of both adsorbents. Additionally, the Frontier Molecular Orbital (FMO) analysis showed that $SiC_{19}$ is more conductive than $C_{20}$. Moreover, the bandgap of $C_{20}$ did not undergo

significant changes during the adsorption process, whereas the bandgap of $SiC_{19}$ decreased from 5.840 (eV) to 3.270 (eV). This indicates that Si-doped fullerene can be utilized as a good electrocatalytic modifier for the electrochemical detection of methyl paraben. In conclusion, the research provides valuable insights into the potential applications of Si-doped fullerenes, particularly $SiC_{19}$, as an effective adsorbent and sensor for the removal and detection of methyl paraben.

## REFERENCES


1. Crovetto SI, Moreno E, Dib AL, Espigares M, Espigares E. Bacterial toxicity testing and antibacterial activity of parabens. Toxicol. Environ. Chem., 2017;99:858-868. https://doi.org/10.1080/02772248.2017.1300905
2. Jonkers N, Sousa A, Galante-Oliveira S, Barroso C, Kohler H-P, Giger W. Occurrence and sources of selected phenolic endocrine disruptors in Ria de Aveiro. Portugal, Environ. Sci. Pollut. Res., 2010;17:834-843. https://doi.org/10.1007/s11356-009-0275-5
3. Steter JR, Rocha RS, Dionisio D, Lanza MRV, Motheo AJ. Electrochemical oxidation route of methyl paraben on a boron-doped diamond anode. Electrochim. Acta, 2014;117:127-133. https://doi.org/10.1016/j.electacta.2013.11.118
4. Dantas RF, Rossiter O, Teixeiraa AKR, Simões ASM, Silva VLD. Direct UV photolysis of propranolol and metronidazole in aqueous solution. Chem. Eng. J., 2010;158(2):143-147. https://doi.org/10.1016/j.cej.2009.12.017
5. Sgroi M, Snyder S, Roccaro P. Comparison of AOPs at pilot scale: energy costs for micro-pollutants oxidation, disinfection by-products formation and pathogens inactivation. Chemosphere, 2021;273:128527. https://doi.org/10.1016/j.chemosphere.2020.128527
6. Dhaka S, Kumar R, Lee SH, Kurade MB, Jeon BH. Degradation of ethyl paraben in aqueous medium using advanced oxidation processes: efficiency evaluation of UV-C supported oxidants. J. Clean. Prod., 2018;180:505-513. https://doi.org/10.1016/j.jclepro.2018.01.197
7. Fang H, Gao Y, Li G, An J, Wong P-K, Fu H, Yao S, Nie X, An T. Advanced oxidation kinetics and mechanism of preservative propylparaben degradation in aqueous suspension of TiO2 and risk assessment of its degradation products. Environ. Sci. Technol., 2013;47:2704-2712. https://doi.org/10.1021/es304898r
8. Gomes JF, Frasson D, Pereira JL, Gonçalves FJM, Castro LM, Quinta- Ferreira RM, Martins RC. Ecotoxicity variation through parabens degradation by single and catalytic ozonation using volcanic rock. Chemical Engineering Journal, 2019;360:30-37. https://doi.org/10.1016/j.cej.2018.11.194
9. Derikvandi H, Nezamzadeh-Ejhieh A. Increased photocatalytic activity of NiO and ZnO in photodegradation of a model drug in aqueous solution: effect of cupling, supporting, particle size and calcination temperature. J. Hazard. Mater.,2017;321:629-638. https://doi.org/10.1016/j.jhazmat.2016.09.056
10. Pipolo M, Gmurek M, Corceiro V, Costa R, Quinta-Ferreira ME, Ledakowicz S, Quinta-Ferreira RM, Martins RC. Ozone-based technologies for parabens removal from water: Toxicity assessment. Ozone Sci. Eng., 2017;39:233-243. https://doi.org/10.1080/01919512.2017.1301246
11. Martins RC, Gmurek M, Rossi AF, Corceiro V, Costa R, Quinta-Ferreira ME, Ledakowicz S, Quinta-Ferreira RM. Application of Fenton oxidation to reduce the toxicity of mixed parabens. Water Sci. Technol., 2016;74:1687-1875. https://doi.org/10.2166/wst.2016.374
12. Safari GH, Nasseri S, Mahvi AH, Yaghmaeian K, Nabizadeh R, Alimohammadi M. Optimization of sonochemical degradation of tetracycline in aqueous solution using sono-activated persulfate process. J. Environ. Health Sci. Eng., 2015;13:76. https://doi.org/10.1186/s40201-015-0234-7
13. Foureaux AFS, Reis EO, Lebron Y, Moreira V, Santos LV, Amaral MS, Lange LC. Rejection of pharmaceutical compounds from surface water by nanofiltration and reverse osmosis. Sep. Purif. Technol.,2019;212:171-179. https://doi.org/10.1016/j.seppur.2018.11.018
14. Zhu J, Lu Z, Jing X, Wang X, Liu Q, Wu L. Adsorption of temozolomide chemotherapy drug on the pristine BC3NT: quantum chemical study. Chem Pap, 2020;74:4525-4531. https://doi.org/10.1007/s11696-020-01232-z
15. Zhao H, Hou S, Zhao X, Liu D. Adsorption and pH-responsive release of tinidazole on metal-organic framework CAU-1. J Chem Eng Data, 2019;64:1851-1858. https://doi.org/10.1021/acs.jced.9b00106
16. Miller TW, Siringan FP, Tanabe S. Determination of preservative and antimicrobial compounds in fish from Manila Bay, Philippines using ultra high performance liquid chromatography tandem mass spectrometry, and assessment of human dietary exposure. J. Hazard. Mater., 2011;192 (3):1739-1745. https://doi.org/10.1016/j.jhazmat.2011.07.006
17. Alnajjar A, AbuSeada HH, Idris AM. Capillary electrophoresis for the determination of norfloxacin and tinidazole in pharmaceuticals with multi-response optimization. Talanta, 2007;72(2):842-6. https://doi.org/10.1016/j.talanta.2006.11.025
18. Lopez-Darias J, Pino V, Meng Y, Anderson JL, Afonso AM. Utilization of a benzyl functionalized polymeric ionic liquid for the sensitive determination of polycyclic aromatic hydrocarbons; parabens and alkylphenols in waters using solid phase microextraction coupled to gas chromatography-flame ionization detection. J. Chromatogr. A., 2010;1217(46):7189-7197. https://doi.org/10.1016/j.chroma.2010.09.016
19. Ioannidi A, Frontistis Z, Mantzavinos D. Destruction of propyl paraben by persulfate activated with UV-A light emitting diodes. J. Environ. Chem. Eng., 2018;6:2992-2997. https://doi.org/10.1016/j.jece.2018.04.049
20. Goyal RN, Rana ARS, Chasta H. Electrochemical sensor for the sensitive determination of norfloxacin in human urine and pharmaceuticals. Bioelectrochemistry, 2012;83:46-51. https://doi.org/10.1016/j.bioelechem.2011.08.006
21. Privett BJ, Shin JH, Schoenfisch MH. Electrochemical Sensors. Anal. Chem., 2010;82(12):4723-41. https://doi.org/10.1021/ac101075n
22. Radovan C, Cinghită D, Manea F, Mincea M, Cofan C, Ostafe V. Electrochemical sensing and assessment of parabens in hydro-alcoholic solutions and water using a boron-doped diamond electrode. Sensors, 2008;8(7):4330-4349. https://doi.org/10.3390/s8074330
23. Hamnca S, Phelane L, Iwuoha E, Baker P. Electrochemical

Determination of Neomycin and Norfloxacin at a Novel Polymer Nanocomposite Electrode in Aqueous Solution. Anal. Lett., 2017;50(12):1887-96. https://doi.org/10.1080/00032719.2016.1261876
24. Jalali Sarvestani MR, Majedi S. A DFT study on the interaction of alprazolam with fullerene (C20). Chem Lett.,2020;1:32-38.
25. Doroudi Z, Jalali Sarvestani MR. Boron nitride nanocone as an adsorbent and senor for Ampicillin: a computational study. Chem Rev Lett., 2020;3:110-116.
26. Ahmadi R, Jalali Sarvestani MR. Adsorption of Tetranitrocarbazole on the Surface of Six Carbon-Based Nanostructures: A Density Functional Theory Investigation. Russ. J. Phys. Chem. B., 2020;14(1):198-208. https://doi.org/10.1134/S1990793120010194
27. Shahzad H, Ahmadi R, Adhami F, Najafpour J. Adsorption of Cytarabine on the Surface of Fullerene C20: A Comprehensive DFT Study. Eurasian Chem Commun, 2020;2:162-169. https://doi.org/10.33945/SAMI/ECC.2020.2.1
28. Tang C, Zhu W, Zou H, Zhang A, Gong J, Tao C (2012) Density functional study on the electronic properties, polarizabilities, NICS values, and absorption spectra of fluorinated fullerene derivative C60F17CF3. Comput Theor Chem., 2012;991:154-160. https://doi.org/10.1016/j.comptc.2012.04.015
29. Elhaes H, Ibrahim M. Fullerene as sensor for halides: modeling approach. J Comput Theor Nanosci., 2013;10:2026-2028. https://doi.org/10.1166/jctn.2013.3164
30. GaussView, Version 6.1, Dennington R, Todd K, and John M. Semichem Inc., Shawnee Mission, KS, 2016.
31. Melchor S, Dobado JA. CoNTube: An Algorithm for Connecting Two Arbitrary Carbon Nanotubes. Journal of Chemical Information and Computing Science, 2004;44(5):1639-1646. https://doi.org/10.1021/ci049857w
32. Gaussian 16, Revision B.01, Frisch MJ, Trucks GW, Schlegel HB, Scuseria GE, Robb MA, Cheeseman JR, Scalmani G, Barone V, Petersson GA, Nakatsuji H, Li X, Caricato M, Marenich AV, Bloino J, Janesko BG, Gomperts R, Mennucci B, Hratchian HP, Ortiz JV, Izmaylov AF, Sonnenberg JL, Williams-Young D, Ding F, Lipparini F, Egidi F, Goings J, Peng B, Petrone A, Henderson T, Ranasinghe D, Zakrzewski VG, Gao J, Rega N, Zheng G, Liang W, Hada M, Ehara M, Toyota K, Fukuda R, Hasegawa J, Ishida M, Nakajima T, Honda Y, Kitao O, Nakai H, Vreven T, Throssell K, Montgomery Jr, Peralta JA, Ogliaro JE, Bearpark F, Heyd MJ, Brothers JJ, Kudin EN, Staroverov KN, Keith VN, Kobayashi TA, Normand R, Raghavachari J, Rendell K, Burant AP, Iyengar JC, Tomasi SS, Cossi J, Millam M, Klene JM, Adamo M, Cammi C, Ochterski R, Martin JW, Morokuma RL, Farkas K, Foresman O, Fox JB, Gaussian, DJ. Inc., Wallingford CT, 2016; GaussView 5.0. Wallingford, E.U.A.
33. Hassani, B., Karimian, M., Ghoreishi Amin, N. DFT Studies on 10 Chromenes Derivatives Performance as Sensing Materials for Electrochemical Detection of Lithium (I). Int. J. New. Chem., 2024; 11(3): 204-215.
34. Tayebi-Moghaddam S, Aliakbari M, Tayeboun K. Fullerene (C24) as a Potential Sensor for the Detection of Acrylamide: A DFT study. Int. J. New. Chem.,2023;11(2):82-89.
35. Rezaei Sameti M, Barandisheh Naghibi M. A quantum assessment of the interaction between Si12C12, BSi11C12, BSi12C11, NSi11C12 and NSi12C11 nanocages with Glycine amino acid: A DFT, TD-DFT and AIM study. Int. J. New. Chem., 2024;11(1):15-33.
36. Abrahi Vahed S, Hemmati Tirabadi F.Carbon Nanocone as a Potential Adsorbent and Sensor for the Removal and Detection of Ciprofloxacin: DFT Studies. Int. J. New. Chem., 2023;10(4):288-298. https://doi.org/10.22034/ijnc.2023.706140
37. Mohammad Alipour F, Babazadeh M, Vessally E, Hosseinian A, Delir Kheirollahi Nezhad P. Theoretical study of some graphene-Like nanoparticles as the anodes in K–ion Batteries. Int. J. New. Chem., 2023;10(3):197-212. https://doi.org/10.22034/ijnc.2022.552410.1295
38. Farahani R, Madrakian T, Afkhami A. Investigating the performance of a recently synthesized covalent organic framework as an adsorbent for methylene blue: A DFT Study. Int. J. New. Chem., 2023;9(4):383-392. https://doi.org/10.22034/ijnc.2023.706008
39. Takano Y, Houk KN. Benchmarking the conductor-like polarizable continuum model (CPCM) for aqueous solvation free energies of neutral and ionic organic molecules. Journal of Chemical Theory and Computation, 2005;1(1):70-77. https://doi.org/10.1021/ct049977a
40. Jalali Sarvestani MR, Abrahi Vahed S, Ahmadi R. Cefalexin adsorption on the surface of pristine and Al-doped boron nitride nanocages (B12N12 and AlB11N12): A theoretical study. S. Afr. J. Chem. Eng., 2024; 47:60-66. https://doi.org/10.1016/j.sajce.2023.10.008
41. Jalali Sarvestani MR, Qomi M, Arabi S. Norfloxacin Adsorption on the Surface of B12N12 and Al12N12 Nanoclusters: A Comparative DFT Study Nanomed. Res. J., 2023; 8(4), 393-400.
42. Jalali Sarvestani MR, Doroudi Z. Tinidazole Adsorption on the Surface of Pristine and Al-Doped Boron Nitride Nanocages: A Comprehensive Theoretical Study Russ. J. Phys. Chem. A., 2023;97(6):1282-1289. https://doi.org/10.1134/S0036024423060195
43. Jalali Sarvestani MR, Doroudi Z. Alprazolam Adsorption on the Surface of Boron Nitride Nanocage (B12N12): A DFT Investigation Russ. J. Phys. Chem. A., 2021;95(Suppl 2):S338 S345. https://doi.org/10.1134/S0036024421150231
44. Jalali Sarvestani MR, Doroudi Z, Ahmadi R. Picric Acid Adsorption on the Surface of Pristine and Al-doped Boron Nitride Nanocluster: a Comprehensive Theoretical Study Russ. J. Phys. Chem. B., 2022;16(1):185-196. https://doi.org/10.1134/S1990793122010286
45. Beheshtian J, Kamfiroozi M, Bagheri Z, Peyghan AA. B12N12 Nano-cage as Potential Sensor for NO2 Detection. Chinese. J. Chem. Phys., 2012;25(1):60-64. https://doi.org/10.1088/1674-0068/25/01/60-64
46. Shakerzadeh E. A DFT study on the formaldehyde (H2CO and (H2CO)2) monitoring using pristine B12N12 nanocluster. Physica E Low Dimens. Syst. Nanostruct., 2016;78:1-9.chttps://doi.org/10.1016/j.physe.2015.11.038